Scientific Reports

https://doi.org/10.1038/s41598-026-38652-y

Article in Press

Land surface phenometrics and their responses to climatic variables in the semi-arid rangelands of the central Zagros mountains

Received: 24 July 2025

Accepted: 30 January 2026

Published online: 09 February 2026

Cite this article as: Pordel F., Jafari R., Esfahani M.T. *et al.* Land surface phenometrics and their responses to climatic variables in the semi-arid rangelands of the central Zagros mountains. *Sci Rep* (2026). https://doi.org/10.1038/s41598-026-38652-y

Fatemeh Pordel, Reza Jafari, Mostafa Tarkesh Esfahani, Mohsen Ahmadi, Geoffrey M. Henebry, Ataollah Ebrahimi, Adrià Descals & Josep Penuelas

Land surface phenometrics and their responses to climatic variables in the semi-arid rangelands of the Central Zagros Mountains

Fatemeh Pordel [a, e], Reza Jafari [a]*, Mostafa Tarkesh Esfahani [a], Mohsen Ahmadi [a], Geoffrey M. Henebry [b, c], Ataollah Ebrahimi [d], Adrià Descals [e, f], Josep Penuelas [e, f]

[a] Department of Natural Resources, Isfahan University of Technology, Isfahan 8415683111, Iran

[b] Department of Geography, Environment, and Spatial Sciences, Michigan State University, East Lansing, MI 48824, USA

[c] Center for Global Change and Earth Observations, Michigan State University, East Lansing, MI 48823, USA

[d] Faculty of Natural Resources and Earth Sciences, Shahrekord University, Chaharmahal va Bakhtiari, Iran

[e] CSIC, Global Ecology Unit CREAF-CSIC-UAB, Barcelona, Spain

[f] CREAF, Cerdanyola del Vallès, Barcelona, Spain

* Corresponding author, Email address: reza.jafari@iut.ac.ir

Abstract

As climate change accelerates, phenological shifts in vulnerable semi-arid ecosystems remain poorly understood yet are of increasingly critical. Identifying the phenological stages of rangeland ecosystems, and quantifying how climate change affects each stage over time, is essential for effective rangeland management. This study aimed to investigate the long-term trends in land surface phenology (LSP) and the impact of climate variations on LSP in the semi-arid rangelands of Chaharmahal-Va-Bakhtiari (CVB) Province, Iran, from 2000 to 2023. Utilizing satellite data from MODIS NDVI, key LSP metrics were analyzed, including the start of the growing season (SOS), peak of the growing season (POS), end of the growing season (EOS), length of the growing season (LOS), and maximum vegetation greenness (maxNDVI). The findings indicate significant shifts: SOS, POS and EOS are occurring earlier, resulting in shorter growing season in many regions. These changes show strong correlations with climatic variables such as precipitation, temperature, and potential evapotranspiration, with temperature exhibiting the most significant relationship to changes in SOS. The Sen's slope trend analysis showed that 25.74% of the study area experienced advancements in SOS, 23.2% % in POS, and 32.3% in EOS. Additionally, LOS has decreased in 70% of pixels with significant change. This study demonstrates that phenological patterns in the semi-arid rangelands of CVB are shifting in response to climate change. These findings highlight the need to implement adaptive management strategies to maintain the sustainability of these fragile ecosystems.

Keywords: Rangeland phenology, MODIS NDVI, phenological metrics, LSP trend

1. Introduction

Land surface phenology (LSP) is the seasonal pattern of changes in vegetated land surfaces detected using remote sensing [1,2]. LSP differs from traditional definitions of plant phenology, which describe specific life cycle events such as flowering, fruiting or leaf fall of individual plants or species using visual observation methods. Thus, LSP is related to but distinct from organismal phenology. Trends in LSP can be obtained by the analysis of satellite time-series data. The LSP can be significantly influenced by climate variables such as air temperature, precipitation, sun radiation, and wind speed [3]. Observing shifts in plant life cycle stages, often stimulated and driven by climatic factors can provide a clearer understanding of how ecosystems react to climate changes. LSP has been significantly affected by climate change in recent decades due to global warming and changes in rainfall seasonality [4], Consequently, it serves a crucial role in the dynamics of terrestrial ecosystems [5]. Start of the growing season (SOS), end of the growing season (EOS), peak of the growing season (POS), and length of the growing season (LOS), are phenological metrics (phenometrics) commonly used to evaluate land surface phenology. Climate change has a major effect on the SOS and EOS with global warming contributing to early spring green-up dates recorded in recent decades in the Northern Hemisphere [6-8] and average lengthening of the growing season globally during 1982–2012 [9]. Similar shifts have also been reported in semi-arid ecosystems outside of Iran, for example in northern China where SOS has advanced and EOS has been delayed in response to changes in precipitation and temperature [10]. Likewise, studies in Xinjiang grasslands in China have documented an advancement of the greening phase by about 5.5 days per decade and a delay in the yellowing phase by about 6.6 days per decade [11].

Few studies on LSP have focused on arid and semi-arid rangelands in Iran [12]. In a study of the Karun River riparian forest in Iran (2000-2020), Sharif and Attarchi [13] analyzed the response of LSP to climatic and edaphic factors, namely precipitation, land surface temperature (LST), and soil salinity. The researchers found a significant decreasing trend in the SOS, POS, and EOS

phenometrics over the study period. EOS showed a strong correlation with mean temperature in Hyrcanian forests of Iran and SOS had a correlation with total precipitation and mean temperature during 1981-2012 [14]. Generally, Hyrcanian forests have exhibited shifts to earlier SOS and later EOS. Global spatial distribution patterns in the Northern Hemisphere showed earlier dates of POS and EOS between 1982 and 2018 [15]. Semi-arid rangelands in Iran play a crucial role in supporting livestock by providing forage and a variety of ecosystem services [16]. Measuring LSP metrics provides critical insights into land surface characteristics and ecos ystem services [17,18]. This information is essential for understanding how semi-arid rangelands can continue to deliver ecosystem services in the future [19,20]. Despite the importance of LSP in rangelands, there have been few studies conducted in Iran's rangelands. For example, a study by Alimoradi, et al. [21] indicated that vegetation cover dynamics in Khouzestan province had a negative correlation with LST and a positive correlation with precipitation. Analyzing trends in LSP can help improve rangeland conditions and assist natural resource managers in mitigating the negative consequences of global warming. Although the extraction of LSP metrics from satellite data is increasing, obtaining accurate measurements in semi-arid regions remains challenging due to low vegetation greenness, extensive soil exposure, and high species diversity [22]. The moderate resolution imaging spectroradiometer (MODIS) has been widely used for LSP studies due to its provision of daily images at medium spatial resolution and global coverage from 2000 to the present [23]. Key phenometrics such as SOS and EOS are fundamental to defining LSP based on remote sensing vegetation indices (VIs), such as the normalized difference vegetation index (NDVI) [24]. These metrics facilitate the characterization of phenological patterns over time [25].

The semi-arid rangelands of Chaharmahal-Va-Bakhtiari (CVB) province are rich and diverse, having been designated as a biosphere reserve by the United Nations Educational, Scientific and Cultural Organization (UNESCO)

in 2015 [26]. Despite their richness and diversity, the semi-arid rangelands of CVB are fragile ecosystems, largely due to the impacts of intensive human activities and climate change [27,28]. Therefore, a comprehensive ecosystem-based study investigating environmental changes in this sensitive ecosystem is essential for land stability and effective management planning. In the current research, we assessed LSP as a suite of ecological indicators to detect environmental changes in the region and its association with topography and climate change, adopting an ecosystem perspective. We hypothesized that changes in peak greenness and phenometrics derived from MODIS would show significant temporal trends, and that these trends would be significantly associated with topographic and climatic variables. The objectives of this study were: 1) to extract phenometrics (SOS, EOS, POS, LOS) from MODIS time series data; 2) to analyze trends in the maximum vegetation greenness (maxNDVI) and phenometrics from 2000 to 2023, and 3) to examine the relationships between phenometrics and both elevation and climatic factors.

2. Materials and methods

2.1. Study area

The southwest province of CVB in Iran served as the research site for this study located between 31° 9′-32° 48′ N- 49° 30′-51° 26′ E (Figure 1). This province is situated among 843-4005 m above sea level. Approximately 10930 km^2, or roughly 55% of the total area, are rangelands. Rangelands in the Zagros Mountains—characterized by grasses, forbs, and shrubs—were masked using the land use / land cover map obtained from the Natural Resources and Watershed Management Administration of CVB. In the northwest region (Koohrang), the average annual precipitation is almost 1400 mm, but in the southern regions (Broujen), it is less than 250 mm. The northwest mountainous regions get cool temperatures, averaging 9 °C, whereas the southern lowlands experience mild temperatures, averaging 15°C. More than 1200 rangeland species have been identified in the study

area. Various species of the genus *Astragalus spp*. are present as the main species in 52 vegetation types and as accompanying species in other vegetation types. The dominant vegetation cover in the study area includes shrubs and annual forbs. Based on climatic classification using a multivariate statistical method, this province is divided into five climatic regions: semi-humid and cold, mountainous cold and very humid, warm and semi-humid, humid and moderate, and semi-arid and cold [29].

Figure. 1. (a) Location of Chaharmahal-Va-Bakhtiari (CVB) province in Iran; (b) climatic classification map showing different climate zones**:** MCVH (mountainous cold and very humid), SHC (semi-humid and cold), SAC (semi-arid and cold), HM (humid and moderate), and WSH (warm and semi-humid); (c) an elevation map (rangelands filled with white colour); and (d) a sample photo of vegetation cover within the study area (Maps were generated using ArcMap 10.5).

2.2. Satellite and climate data

The NDVI data for vegetated cover areas were extracted from the MODIS Collection 6.1 MOD13Q1 product. This dataset for the study area spans 18 February 2000 to 31 December 2023, yielding a total of 545 composite images. The study area lies entirely within a single MODIS tile (h26v05), so only one tile was required to ensure complete spatial coverage. The MOD13Q1 product has been consistently available since early 2000, offering the longest continuous NDVI record at 250 m spatial resolution. This product was provided by the National Aeronautics and Space Administration Land Processes Distributed Active Archive Center (NASA LP DAAC) at the United States Geological Survey Earth Resources Observation and Science (USGS EROS) Center (https://lpdaac.usgs.gov/data/). ECMWF Reanalysis v5 (ERA5) data, which is a reanalysis dataset produced by the European Centre for medium-range weather forecasts (ECMWF) were downloaded for the period 2000-2023 (https://cds.climate.copernicus.eu/datasets/reanalysis-era5-singlelevels?tab=overview). It provides global atmospheric reanalysis data

covering the period from 1950 to the present at a high temporal (hourly) and spatial resolution (0.25° × 0.25°). Pre-SOS mean potential evapotranspiration (PET), pre-SOS mean temperature, and pre-SOS total precipitation were collected using google earth engine (GEE) to correlate with the SOS. These variables were calculated for 40 days before the SOS for each pixel to capture pre-SOS environmental conditions influencing the SOS. Additionally, data on growing season (GS) PET, GS temperature, GS precipitation, pre-EOS mean PET, pre-EOS mean temperature, and pre-EOS total precipitation were gathered using GEE to correlate with the EOS. Data on GS PET, GS temperature, and GS precipitation were also calculated for each pixel during the GS and their correlation with the EOS was examined. Furthermore, pre-EOS mean PET, pre-EOS mean temperature, and pre-EOS total precipitation were calculated for the 40 days before the EOS to assess pre-season conditions leading up to the EOS.

2.3. Extraction of phenometrics

Clouds, aerosols, compositing artifacts, and other sources of noise can cause outliers in vegetation index (VI) values. Therefore, it is necessary to pre-process the NDVI time series data to reduce sources of high frequency variation. In LSP studies, time series smoothing is necessary to enhance the precision of phenology estimation before calculation of the phenometrics. Time series de-noising generally applies multiple smoothing techniques such as Savitzky-Golay filter [30,31], logistic function [17], and the asymmetric Gaussian function fitting [32]. Some researchers used other smoothing methods to reconstruct VI time series in addition to these three main techniques, such as harmonic analysis of time series (HANTS) algorithms [33] and median filters [34]. In the current study, quality assurance (QA) flags in the pixel reliability band were used to filter out poor-quality retrievals (2 and 3 QA values). After that, time-series gap filling (TSGF) using spline interpolation to reconstruct

missing data points was applied to fill gaps in a time series and smooth the time series.

Four types of LSP characterization techniques exist: threshold-based, derivative-based, smoothing functions, and fitted models techniques [35]. In the last step, the phenometrics, such as the SOS and EOS, were derived from the daily, weekly, or monthly time series that have been interpolated, smoothed, and gap-filled. The threshold method was used to determine the SOS, EOS and LOS as EOS-SOS+1. The green-brown package in R and ArcMap 10.5 software were used to analyze the time series of MOD13Q1 NDVI and extract SOS, EOS, POS, and LOS maps from 2000 to 2023 [36].

2.4. Trend analysis of LSP metrics and maxNDVI

This study extracted the trends of LSP metrics and maxNDVI from 2000 to 2023 in the study area using the Mann-Kendall analysis [37]. The Theil-Sen median analysis and the Mann-Kendall non-parametric statistical test used to detect significant trends in a time series of data, without requiring the data to follow normal distribution. The Theil-Sen analysis provides a robust estimate of the trend slope by taking the median of all pairwise slopes between data points, which is resistant to outliers and non-normal distributions. This test has multiple parameters, and in this study, the Sen's slope parameter to quantify the magnitude of the trend was used:

$$\text{Sen's slope} = \text{median}\left(\frac{x_j - x_i}{j - i}\right) \quad (1)$$

Where, Sen's slope indicates the rate of change per time unit. x_j and x_i are date values (date of the growing season or value of maxNDVI) at time *j* and *i* Slope > 0 indicates an increasing trend, while the opposite indicates a decreasing trend, and the larger the absolute value, the more pronounced the trend. A significance level of p-value ≤ 0.05 was used to distinguish statistically significant trends [38].

2.5. Correlation analysis between LSP and climatic variables

2.5.1. Kendall's correlation coefficient (τ)

Kendall's tau (τ) is a non-parametric correlation coefficient used to measure the strength and direction of association between two ranked variables. Unlike Pearson's correlation, which assesses linear relationships, Kendall's tau evaluates ordinal associations, making it robust to outliers and applicable to non-normally distributed data[1]. We opted for the Kendall correlation test instead of the Spearman test although both are non-parametric since Kendall's method offers greater robustness against deviations from normality [39]. Mathematically, Kendall's tau is defined as:

$$\tau = \frac{C - D}{C + D} \quad (2)$$

where, C represents the number of concordant pairs, where the rankings of both variables move in the same direction and D represents the number of discordant pairs, where the rankings move in opposite directions. In cases where tied values exist, a modified formula is used:

$$\tau = \frac{C - D}{\sqrt{(C + D + \tau_{\chi})(C + D + \tau_{\square})}} \quad (3)$$

where τ_{χ} and $\tau_{\square}$ denote the number of tied values in variables x and y, respectively. Kendall's tau values range from -1 to +1, where $\tau = 1$ indicates a perfect positive correlation, $\tau = -1$ indicates a perfect negative correlation, and $\tau = 0$ implies no correlation between the variables.

2.5.2. Kruskal-Wallis test

The Kruskal-Wallis test follows a rank-based approach to compare three or more independent groups. In data ranking, all observations are combined and ranked in ascending order, with tied values assigned average ranks [40].

$$H = \frac{12}{N(N+1)} \Sigma \frac{R_i^2}{N_i} - 3(N+1) \quad (4)$$

Where N is the total number of observations, R_i is the sum of ranks for group i, and N_i is the number of observations in group i. If H is small, this suggests that the groups have similar rank distributions and there is no significant difference among them. Conversely, if H is large, it indicates that at least one group differs significantly. It is important to note that the size of H depends on the number of groups (k) and the sample size (N), and there is no fixed threshold for what constitutes a "big" or "small" H. For a given significance level ($\alpha = 0.05$), we compare H to the chi-square critical value. If H exceeds this value, we conclude that at least one group differs significantly.

3. Results

Overall, our results revealed clear Spatial-temporal patterns in vegetation phenology across the study area from 2000 to 2023. Multi-year averages of SOS, POS, EOS and LOS showed strong elevational and climatic gradients, with lower elevations exhibiting earlier phenological events and longer LOS. Trend analyses using Sen's slope and the Mann-Kendall test indicated widespread greening, an advancement of SOS and POS, and mixed but meaningful shifts in the EOS. Correlation analyses further demonstrated that SOS was primarily controlled by pre-SOS mean temperature and pre-SOS accumulated precipitation, whereas EOS responded more strongly to climatic conditions during the growing season.

3.1. Maps of phenometrics

Figure 2 presents spatial distribution maps of the multi-year average phenometrics from 2000 to 2023, represented as day of the year (DOY). Each class in Figure 2 corresponds to a quartile of the numerical value range depicted in the map. Figure 3 contains charts, likely showing variations in

SOS, POS, EOS and LOS across different elevational classes and climatic zones using the Kruskal-Wallis test. Phenometrics exhibited a clear elevation pattern with each group showing a significant difference (p-value ≤ 0.05). The mean SOS was in the range of DOY 30 to DOY 180, with 46% of pixels falling between DOY 30 and DOY 68, i.e., end of January to early March (Figure 2a). Generally, earlier SOS dates were mainly distributed at lower elevations (Figure 3a). DOY 106 to DOY 143, i.e., mid-April to third week of May, were observed in higher elevation areas (2900- 3500 m) (Figure 3a). The last category (DOY 144 to DOY 180), with the most delayed SOS, accounted for 1% of the total area at elevations above 3500 meters. Figure 3 a clearly shows that with increasing elevation, the median DOY of SOS increases. The mean value of POS ranged from DOY 90 to DOY 240. POS occurred in 64% of the pixels in the study area within the 129th-165th DOY category, from early April to mid-June. These areas were mostly located in the eastern part of the region and corresponded to areas where the SOS was DOY 30 and DOY 105. As shown in Figure 2a-b, in areas where the SOS occurred later, POS also fell into categories with higher values. Like SOS, POS showed clear spatial heterogeneity; the distribution of vegetation greening peak period was significantly influenced by elevation and with increasing elevation, the SOS and POS occurred later (Figure 3a). During the dry stage, the mean EOS ranged widely from DOY 100 to DOY 270 (Figure 2c). In the study area, 59% of the pixels had EOS between DOY 186 to 228, from early July to mid-August. These areas were mostly located in the eastern part of the study area. In most of these areas, the POS occurred between DOY 129 and DOY 165. Approximately 23% of the pixels are in the 229th-270th day of the year category, corresponding to mid-August to late September. The average LOS ranged from 70 to 215 days, and 51% of the pixels in the study area, had a LOS between 144 and 180 days (Figure 2d). The lowest elevation category had the longest average LOS, with an average value of 150 days (Figure 3a). Lower elevation areas experienced fewer environmental constraints on plant growth, allowing for a longer growing season, when

water is available. Not surprisingly, the shortest LOS corresponds to the highest elevation range (3500-4174 m). The humid and moderate climatic zones exhibited the greatest variability in all LSP metrics, showing the highest average in the SOS and POS compared to other climatic zones. Subsequently, the rank order for average SOS and POS, from highest to lowest, was as follows: mountainous cold and very humid, semi-humid and cold, semi-arid and cold, and warm and semi-humid. The semi-arid and cold, semi-humid and cold climatic zones exhibited lower variation. In terms of EOS, the order of average values was mountainous cold and very humid, semi-arid and cold, semi-humid and cold, warm and semi-humid, and humid and moderate climatic zones. For LOS, the mountainous cold and very humid zone had longer averages, while the duration in other climatic zones was nearly equal (Figure 3b).

Figure. 2. Spatial distribution of average phenometrics from 2000 to 2023 reported on day of the year (DOY) ranges for (a) start of the growing season (SOS), (b) peak of the growing season (POS), (c) end of the growing season (EOS), and (d) length of the growing season (LOS). Each class represents one quartile of the range of numerical values in the map. Areas without rangelands filled with gray colour (Maps were generated using ArcMap 10.5).

Figure. 3. Evaluating the influence of (a) elevation and (b) climatic zone on the average of phenometrics from 2000 to 2023 (a Kruskal-Wallis analysis of start of the growing season (SOS), peak of the growing season (POS), end of the growing season (EOS), and length of the growing season (LOS) with p-value ≤ 0.05). The line inside each box represents the median, while the bottom and top of the box indicate the first quartile and third quartile, respectively.

3.2. Nonparametric trend analyses of ΔmaxNDVI and phenometrics

Nonparametric trends at pixel scale were estimated using Sen's slope to estimate trend magnitudes and directions and the Mann-Kendall test to calculate the exact significance levels for NDVI from 2000 to 2023. The most significantly increases in NDVI values were observed around rivers and

wetlands. However, overall, Sen's slope trends did not reveal a clear elevational pattern across more than half of the study area. The results showed that 74% of the pixels (representing 98.6% of significantly changed pixels) exhibited a significant positive increase in ΔmaxNDVI at a 95% confidence level (p-value ≤ 0.05), indicating enhanced vegetation cover. In contrast, only 1.33% of significantly changed pixels displayed a significantly negative trend. 25% of the pixels showed no significant changes (p-value > 0.05), suggesting stable vegetation conditions in terms of greenness between 2000 and 2023 (Figure 4a).

The inter-annual variability of SOS, POS, EOS, and LOS in the study area from 2000 to 2023 have shown notable trends over the past 24 years (Figure 4b-e). Sen's slope analysis of the LSP metrics revealed significant changes in SOS for 26% of the pixels in the study area (p-value ≤ 0.05) (Figure 4b), with 99% of these pixels indicating an advanced trend in SOS and 1% of these pixels indicating delayed trend from 2000 to 2023. According to Figure 4c, the slope trend values for POS indicated a significantly change for 24% of the pixels, while 76% showed no significant change. Among the pixels with significant changes, 97% exhibited an earlier occurrence of POS and 3% exhibited later. The spatial distribution of slope trends for SOS and POS was relatively similar. Additionally, trends of advancement and delay were observed throughout the entire area without following a defined pattern. The results indicate that 34% of the pixels in the study area experienced significant changes in EOS. A significant majority of pixels (95%) showed a negative trend in the EOS, signaling an earlier occurrence, while the remaining 5% exhibited a positive trend, suggesting a delay. Furthermore, significant changes were observed in the LOS for 28% of pixels. The negative Sen's slope for LOS indicated a shortening of the growing season in 70% of the pixels, whereas 30% indicated a lengthening of the growing season with significant changes from 2000 to 2023.

Figure 5 illustrates that the median Sen's slope trends for NDVI for all elevational classes were positive. The median Sen's slope trends for SOS and POS were negative, indicating an advancement in these parameters during 2000 to 2023. The median Sen's slope trends in EOS were negative for the first three elevational classes, while the two highest elevational classes were close to zero. In the first and second elevational classes (792–2000 m), the median Sen's slope trend for LOS was positive, while it was negative in the 2000–2900 m range. In the highest elevational classes (2900–3500 m and 3500–4174 m), the median Sen's slope trend in LOS was close to zero.

Figure. 4. Spatial-temporal slope trends of phenology metrics from 2000 to 2023: (a) max- NDVI, (b) start of the growing season (SOS), (c) peak of the growing season (POS), (d) end of the growing season (EOS), and (e) length of the growing season (LOS). Areas without rangelands appear white (Maps were generated using ArcMap 10.5)..

Figure. 5. Elevation- based Kruskal-Wallis analysis of Sen's slope for NDVI, start of the growing season (SOS), peak of the growing season (POS), end of the growing season (EOS), and length of the growing season (LOS) (p-value ≤ 0.05). The line inside each box represents the median, while the bottom and top of the box indicate the first quartile and third quartile, respectively.

3.3. SOS response to climatic variables

The SOS showed a significantly positive correlation with pre-SOS accumulated precipitation in 45% of pixels, reaching a significance level of p-value ≤ 0.05 (Figure 6a), meaning more precipitation accumulated in the pre-SOS period delayed the start of the growing season. The correlation between the SOS and pre-SOS accumulated precipitation showed a stronger correlation in most areas at elevations > 2900 m (Figure 7). Overall, in areas with a significant relationship with increasing elevation, the correlation between SOS and pre-SOS accumulated precipitation increased. There was a significant negative correlation between SOS and pre-SOS mean

temperature in 72% of pixels (p-value ≤ 0.05) (Figure 6b). It means that the increase in pre-SOS mean temperature leads to earlier vegetation greening in the study area. The median correlation in all the correlation classes was negative (Figure 7). It is important to note that the significance or non-significance of the relationship between pre-SOS mean temperature and the SOS does not follow a specific pattern in the study area. For 98% of pixels with significant relationship between SOS and pre-SOS mean temperature, the correlations ranged between -1 and -0.2. The correlation between the SOS and pre-SOS mean PET was negative and significant (p-value ≤ 0.05) in 56% of the study area (Figure 6c), indicating that with an increase in evapotranspiration, the SOS shifted earlier. The correlation in 96% pixels with significant relationship ranged between -0.8 and -0.2. As temperature increases, so does evapotranspiration; therefore, an increase in pre-SOS mean PET is associated with an earlier SOS. According to the results, the SOS showed a stronger correlation with pre-SOS mean temperature compared to pre-SOS accumulated precipitation and pre-SOS mean PET.

3.4. EOS response to climatic variables

Correlations between EOS timing and two categories of climatic variables were examined: (1) variables measured during the 40 days' period prior to the EOS; and (2) variables measured throughout the growing season (from the start through the end of the growing season). In 96% of the pixels, correlations between EOS and pre-EOS total precipitation were not significant at the 95% confidence level, suggesting that EOS was not sufficiently correlated with pre-EOS total precipitation (Figure 6d), the 792 m to 1450 m elevational class showed stronger median correlation (Figure 7). Additionally, EOS timing was not significantly related to pre-EOS mean temperature in 81% of the pixels, while only 19% of the pixels exhibited a significant correlation with negative values (Figure 6e). This finding indicates that higher pre-EOS mean temperatures led to earlier EOS. The areas of significant correlations were located mostly in the eastern parts, and the

median correlation was stronger at lower elevations (792 m to 1450 m) (Figure 7). There were no significant correlations between EOS and pre-EOS mean PET in 83% of the pixels, and 15% of the pixels displayed a significantly negative correlation and 2% displayed a significantly positive correlation (Figure 6f).

The correlation between EOS and GS precipitation indicated that there was no significantly relationship between these two parameters in 92% of the region. In contrast, 6% of the pixels showed a significantly positive correlation, and 2% displayed a significantly negative correlation. These pixels with positive and negative correlations were distributed throughout the entire region. The median correl ations were positive in the first three elevational classes (from 792 to 2900 m) and negative in the last two elevational classes (from 2900 to 4174m) (Figure 6g). Regarding GS temperature, EOS was not significantly related to GS temperature in 72% of the pixels, whereas 25% exhibited a significantly negative correlation, suggesting that in areas with a significantly negative correlation, the dry stage occurs later when GS temperature is cooler. 3% of the pixels showed significant positive correlation (Figure 6h). EOS was not significantly related to GS PET in 84% of the pixels, whereas 10% showed a significant negative correlation and 6% exhibited a significant positive correlation (Figure 4i). The median was negative across all elevational classes, with the expectation of the last classes, in which it was positive (Figure 7). The first three elevational classes have a positive median while the last two classes have a negative median. Overall, GS PET did not significantly affect the occurrence of the EOS season across most of the region (p-value > 0.05). EOS demonstrated a stronger correlation with climatic parameters in the growing season (GS temperature, GS precipitation and GS PET) compared to pre-EOS mean parameters (pre-EOS mean temperature, pre-EOS total precipitation, pre-EOS mean PET), with temperature in the growing season showing the highest

correlation and significance related to the occurrence of EOS among the variables.

Figure. 6. Spatial distribution of Kendall's correlation coefficient between the land surface phenology (LSP) metrics and climate variables in the study area during 2000-2023: (a) Pre-SOS total precipitation, (b) Pre-SOS mean temperature, (c) Pre-SOS mean PET, (d) Pre-EOS total precipitation, (e) Pre-EOS mean temperature, (f) Pre-EOS mean PET, (g) Growing season precipitation, (h) Growing season temperature, and (i) Growing season PET (Maps were generated using ArcMap 10.5).

Figure. 7. Elevation-based Kruskal-Wallis analysis of Kendall's correlation coefficient between the land surface phenology (LSP) metrics and climate variables in the study area during 2000-2023 (p-value ≤ 0.05). The line inside each box represents the median, while the bottom and top of the box indicate the first quartile and third quartile, respectively.

4. Discussion

Recent studies indicated that temperature increases in Southwest Asia were surpassing the global average [41] . Our findings showed that the MODIS NDVI phenometrics exhibited spatio-temporal changes in the study area from 2000 to 2023, driven by shifts in climatic variables. Specifically, at higher elevations (> 2900 m), environmental constraints- such as cooler temperatures and poorer soil quality-led to later SOS, which in turn contributed to a delayed POS [42]. Additionally, these higher elevation areas also exhibited an earlier occurrence of EOS [43]. The diversity of rangeland species in the study area was very high; this made it impossible to differentiate between species given the relatively coarse spatial resolution of the MODIS NDVI product and the ruggedness of the terrain. Consequently, the analyses were conducted at the scale of the dominant vegetation type rather than at the species level. In areas where the SOS ranged between DOY 68 and DOY 105 and the LOS was long, the dominant species were perennial

grasses, such as *Bromus tomentellus* and *Agropyron desertorum*, shrub species, like *Astragalus gossypinus*, or forbs, such as *Cousinia spp.* These species had a relatively long greening period, which extended their growing season [44]. The increased spatial heterogeneity observed in the EOS map, especially in the eastern and northeastern parts of the region where there were more fine classes per unit area, likely resulted from grazing pressures and the types of utilization. Rangeland utilization affected the persistence of greenness during the growing season, and could vary across areas. For instance, a study by Pordel, et al. [45] reported that areas with controlled grazing exhibited increased stability of plant biomass and greenness.

Soltani, et al. [29] found that the eastern and northeastern parts of the study area fell within semi-humid and cold, as well as semi-arid and cold climates. These areas exhibited greater elevational homogeneity, with an average elevation ranging between 2200 m and 2900 m, where the LSP metrics showed less spatial heterogeneity. For instance, the 30th-68th and 68th-105th classes for the SOS, the 128th-165th class for the POS, the 185th-228th class for the EOS, and the 106-143 and143-180 classes for the LOS constituted the dominant areas in the eastern and northeastern parts. In the humid and moderate climate zone, located in the western and northwestern parts of the region, most rangelands were situated at higher elevations, with notably elevational heterogeneity covering almost all elevational classes. The latest SOS class (from DOY 143 to DOY 180), the latest POS class (DOY 202 to 240), the latest EOS class (DOY 228 to 270), and the shortest growing period (< 106 days), along with the other phenometric classes, were found in this climate zone. Lower elevations in this climate zone were mainly composed of forested areas. Similarly, the mountainous cold and very humid climate zone, located in the northern part of the study area, was associated with highly elevational heterogeneity (a wide range of elevations, 2200 m to 4174 m), where phenometrics showed greater diversity across classes. The timing of phenometrics in different climate zones was influenced not only by

the general temperature and precipitation conditions of each zone but also significantly by elevation within those areas [46]. This elevation factor was crucial and should be considered in management programs related to rangeland utilization.

In a large part of the study area exhibiting significant changes between 2000 and 2023, phenometrics indicated multiple shifts to earlier timings of SOS, POS, and EOS and the LOS became shorter. In regions with significant trends in both SOS and EOS, the unequal magnitude of these shifts ultimately resulted in a negative slope, indicating a shortening of the LOS. These advances in SOS in CVB aligned with projections from IPCC AR6 WGII Chapter 10 for regions such as West Asia, which emphasized significant increases in extreme temperatures, elevated heat stress levels, and increased aridity conditions known to drive phenological alterations in semi-arid ecosystems [47]. Pan, et al. [48] also demonstrated that the SOS in the Northern Hemisphere advanced from 1992 to 2020. In several studies, heavy grazing in certain areas of the study region was reported [49,50]. Additionally, Heidari Ghahfarrokhi, et al. [51] demonstrated that with increasing grazing intensity, the plant community shifted from perennial grasses and forbs toward annual plants. We speculated that the dominance of annual plants due to heavy grazing was a key reason for the earlier SOS timing, because annual plants began growth earlier compared to perennial shrubs and grasses. A phenometric study using finer spatial resolution (i.e., Landsat data) from 2000 to 2020 across multiple countries in Southwest Asia, including Iran, found that the timing of the SOS was significantly influenced by rainfall variability, with increased rainfall leading to delays in SOS. Additionally, this study highlighted a advanced trend in SOS timing in rangelands throughout the region [52]. Another study analyzed the LSP trends of Iran's vegetation using coarse spatial resolution AVHRR data and the NDVI index from 1982 to 2019. They found that the northeastern, western, and northwestern regions of Iran exhibited a negative slope trends, indicating that the SOS had

begun earlier [53]. They also showed that EOS in many parts of Iran, particularly in the west, northwest, and parts of the northeast, had negative slope trends, with EOS occurring approximately 1.33 days earlier each year. These changes in the timing of SOS and EOS attributed to temperature increases caused by climate change. Our findings were consistent with broader evidence from other semi-arid and Mediterranean-type regions. For example, Vogel [54] examined the phenology of deciduous trees, shrubs, and agricultural crops in southern Europe and reported a noticeable acceleration in phenological phases, highlighting vegetation's strong sensitivity to warming trends. Another study focusing on semi-arid regions of the southern Mediterranean, including Morocco, Algeria, and Tunisia, revealed trends similar to those observed in the Zagros Mountains regarding the earlier onset of the growing season. This regional alignment highlighted the importance of understanding phenological changes in semi-arid ecosystems for the sustainable management of rangelands and agriculture [55].

The present study showed that in 45% of the area, an increase in cumulative precipitation before the SOS caused later SOS. The average correlation in most elevational classes ranged between 0.3 and 0.4. In contrast, in 70% of the area, an increase in pre-SOS mean temperature led to earlier greening of the vegetation. The higher elevation regions, particularly in the Zagros Mountains, create specific conditions for plant growth. In these areas, temperatures are generally lower, and the growing periods are shorter compared to the lower elevation plains. These factors cause plants at higher elevations to be more correlated to pre-SOS mean temperatures. Additionally, 56% of the area showed negative correlations between pre-SOS mean PET and the SOS. This relationship indicated that an increase in PET shifted the SOS earlier. The stronger correlation and the higher percentage of significant pixels across the study area indicated that SOS was more strongly correlated with pre-SOS mean temperatures than with precipitation and PET. The relationship between the EOS and climatic variables showed

that pre-EOS total precipitation had no significant effect on 96% of the pixels, indicating that dry stage of plants was not dependent on pre-EOS total precipitation. Pre-EOS mean temperatures also showed no correlation in 81% of the pixels. However, in 19% of the areas, an increase in temperature led to an earlier EOS. These pixels were primarily located in the eastern part of the study region. Pre-EOS mean PET also had no apparent effect in 83% of the pixels, with that only 14% of the pixels showing a significant negative correlation and 6% showing a significantly positive correlation. Similar to pre-EOS mean temperature, the pre-EOS mean PET pixels with a stronger mean correlation were located at elevations between 792 m and 1450 m. Lower elevation areas generally experienced higher temperatures, and in these areas, temperature and evapotranspiration have significantly influenced EOS timing.

GS cumulative precipitation showed no correlation with EOS timing in 92% of the study area. Only 6% and 2% of the pixels exhibited significant positive and negative correlations, respectively. The GS temperature correlated with earlier EOS in 28% of the area, while PET had no effect in 84% of the pixels. Overall, the EOS showed strong correlation to climatic parameters related to the GS (especially temperature). In studies of LSP and climate impact, various regions with uniquely climatic and geographical characteristics had been examined across different parts of the world. Cleland, et al. [6] examined LSP changes on a global scale and found that rising temperatures in the Northern Hemisphere led to earlier greening of plants, aligning with the findings of the present study. Wipf, et al. [56] studied the effects of temperature changes and snow on SOS in the Alpine highlands and concluded that the effects of pre-SOS mean temperature and snowmelt timing in high-elevation areas were complex and depended on the specific plant species. The findings of the present study indicated that the SOS at higher elevations (> 3000 m) showed less sensitivity to pre-SOS mean temperatures, with median correlation close to 0, compared to other areas. The lower sensitivity of SOS

at > 3000 m likely reflects the dominant influence of snowmelt timing, soil thermal constraints, and alpine species' low thermal responsiveness, which together weaken the direct relationship between SOS and pre-SOS mean temperature [57,58] . Garonna, et al. [59] studied the impact of three climatic constraints (minimum temperature, moisture availability, and photoperiod) on phenometrics across eight ecological regions worldwide. They reported a reduced influence of minimum temperature on SOS and EOS in every region. In contrast, the effects of moisture and day length varied depending on the type of biome, but they did not consider the influence of elevation on LSPs. In Iran, Araghi, et al. [12] examined the trends in SOS and EOS between 1982 and 2015 and found that these trends were influenced by various climatic fluctuations. Their results indicated that, under the influence of climatic patterns, the SOS generally began earlier in different regions of Iran.

The result of Sen's slope trend or the difference in the maximum NDVI from 2000 to 2023 showed a significantly positive values of ΔmaxNDVI for nearly three-quarters of the study area. This widespread increase indicated a slight improvement in the vegetation greenness of the study area. Due to overgrazing and vegetation cover destruction, national and international projects were implemented in the study area in recent years to restore the vegetation, including fencing to restrict grazing and seeding. In more recent years, the species *Prangos ferulacea* was planted in the area, notable for its extensive canopy and high greenery. Medicinal plants such as *Ferula assafoetida* and *Apium graveolens* were also cultivated in the region. These factors may explain the observed slight improvement in vegetation greenness; however, overgrazing could also have increased the fraction of unpalatable plants, thereby increasing apparent greenness while reducing forage [60]. More than a quarter of rangelands in the study area showed no significant changes. The unchanged vegetation can guide managers in assessing rangeland conditions for future utilization. For example, areas that have not shown an increase in vegetation cover can be targeted for study,

and if necessary, programs for vegetation restoration, conservation, and grazing-management improvement can be implemented. Considering the early SOS, grazing plans should be adjusted based on changes in the phenological patterns of plants. Preventing overgrazing during periods when vegetation is vulnerable and optimizing grazing timing when plant growth peaks are crucial. Land managers can use this information to implement targeted restoration programs aimed at enhancing the resilience of native vegetation, reestablishing key species, and managing invasive plants that thrive under changing climate. LSP changes can affect the availability of food and habitat for wildlife, especially for species that depend on specific timing for breeding or migration; conservation efforts can focus on preserving species most impacted by these changes. Based on the results, by highlighting which LSP metrics are more sensitive to climate change, relevant organization can prioritize conservation toward areas requiring greater protection.

Despite the robustness of the applied methods, this study is subject to several limitations. First, the spatial resolution of the satellite sensor constrained the derived phenometrics, potentially obscuring fine-scale vegetation dynamics and rapid transitional events. Future studies would benefit from incorporating higher-resolution sensors to better resolve localized phenological patterns. Additionally, accuracy and ecological interpretability could be substantially enhanced by integrating remote sensing data with field-based observations and long-term ecological monitoring programs [61] . Citizen science platforms also offer a valuable source of complementary data for large-scale phenological assessments [62]. A critical research direction is to disentangle the relative contributions of climate change and human management practices to observed phenological shifts, as distinguishing these drivers is essential [63]. Finally, the influence of spatial scale warrants more explicit consideration, as phenological responses are often scale-dependent [64]. Collectively, these advancements

would foster a more comprehensive understanding of vegetation phenology and improve predictions of future ecosystem responses to environmental change.

5. Conclusions

To assess the influence of rising temperatures and other climatic variables on LSP, we analyzed the SOS, POS, EOS, and LOS phenometrics in the semi-arid rangelands of the Zagros Mountains from 2000 to 2023 using MODIS NDVI time-series data. The results aligned with the findings of previous studies and highlighted the dominant role of temperature in driving changes in LSP. Warming led to statistically significant advances in the SOS, POS, and EOS across the majority of the region. LOS was strongly negatively correlated with pre-SOS mean temperature but positively correlated with pre-SOS total precipitation. This pattern suggests that warmer temperatures hasten vegetation growth, while increased precipitation may delay it, possibly due to associated cooling effects. Consequently, warming trends were the primary driver of the shortened LOS, which reduced the effective vegetation growth period. These changes point to the critical role of climate in reshaping vegetation dynamics in mountainous regions. For future studies, it is recommended to utilize high spatial resolution satellite datasets, such as Sentinel-2, to capture greater diversity in LSP spatial patterns in semi-arid terrains with low vegetation greenness.

Acknowledgements

We would like to thank the Department of Natural Resources of Iran, the Global Ecology Unit at CREAF-CSIC-UAB, Barcelona, and the Center for Global Change and Earth Observations at Michigan State University.

Declaration of interest statement

The authors declare that they have no known competing financial interests or personal relationships that could have appeared to influence the work reported in this paper.

Data availability

The datasets generated during the current study are available from the corresponding author on reasonable request.

Funding

The authors received no financial support for the research, authorship, and publication of this article.

References

1 De Beurs, K. M., Driscoll, E. & Henebry, G. M. Land Surface Phenology in Global Change Studies, in: Schwartz, M.D. (Ed.), Phenology: An Integrative Environmental Science. Springer Nature Switzerland, Cham, pp. 505-529. (2024).

2 Henebry, G. M. & De Beurs, K. M. in *Phenology: An Integrative Environmental Science* (ed Mark D. Schwartz) 385-411 (Springer Netherlands, 2013).

3 Wang, L., She, D., Xia, J., Meng, L. & Li, L. Revegetation affects the response of land surface phenology to climate in Loess Plateau, China. *Science of The Total Environment* **860**, 160383, doi:https://doi.org/10.1016/j.scitotenv.2022.160383 (2023).

4 Peñuelas, J. & Filella, I. Phenology. Responses to a warming world. *Science* **294**, 793-795, doi:10.1126/science.1066860 (2001).

5 Gong, Z., Ge, W., Guo, J. & Liu, J. Satellite remote sensing of vegetation phenology: Progress, challenges, and opportunities. *ISPRS Journal of Photogrammetry and Remote Sensing* **217**, 149-164, doi:https://doi.org/10.1016/j.isprsjprs.2024.08.011 (2024).

6 Cleland, E. E., Chuine, I., Menzel, A., Mooney, H. A. & Schwartz, M. D. Shifting plant phenology in response to global change. *Trends in Ecology & Evolution* **22**, 357-365, doi:https://doi.org/10.1016/j.tree.2007.04.003 (2007).

7 Shen, M. *et al.* Can changes in autumn phenology facilitate earlier green-up date of northern vegetation? *Agricultural and Forest Meteorology* **291**, 108077, doi:10.1016/j.agrformet.2020.108077 (2020).

8 Bellini, E. *et al.* Impacts of Climate Change on European Grassland Phenology: A 20-Year Analysis of MODIS Satellite Data. *Remote Sensing* **15**, 218, doi:10.3390/rs15010218 (2023).

9 Garonna, I., de Jong, R. & Schaepman, M. E. Variability and evolution of global land surface phenology over the past three decades (1982–2012). *Global Change Biology* **22**, 1456-1468, doi:https://doi.org/10.1111/gcb.13168 (2016).

10 Song, X., Liao, J., Zhang, S. & Du, H. Land Surface Phenology Response to Climate in Semi-Arid Desertified Areas of Northern China. *Land* **14** (2025).

11 Dong, T. *et al.* Seasonal Scale Climatic Factors on Grassland Phenology in Arid and Semi-Arid Zones. *Land* **13** (2024).

12 Araghi, A., Martinez, C. J., Adamowski, J. & Olesen, J. E. Associations between large-scale climate oscillations and land surface phenology in Iran. *Agricultural and Forest Meteorology* **278**, 107682, doi:https://doi.org/10.1016/j.agrformet.2019.107682 (2019).

13 Sharif, M. & Attarchi, S. Investigating the effect of temperature, precipitation, and soil salinity changes on Riparian Forests' phenology using a remote sensing approach. *Remote Sensing Applications: Society and Environment* **34**, 101194, doi:https://doi.org/10.1016/j.rsase.2024.101194 (2024).

14 Kiapasha, K. *et al.* Trends in Phenological Parameters and Relationship Between Land Surface Phenology and Climate Data in the Hyrcanian Forests of Iran. *IEEE Journal of Selected Topics in Applied Earth Observations and Remote Sensing* **10**, 4961-4970, doi:10.1109/JSTARS.2017.2736938 (2017).

15 Wu, W. *et al.* Developing global annual land surface phenology datasets (1982–2018) from the AVHRR data using multiple phenology retrieval methods. *Ecological Indicators* **150**, 110262, doi:https://doi.org/10.1016/j.ecolind.2023.110262 (2023).

16 Fatemi, S. S., Rahimi, M. & Bernardi, M. The most important climatic factors affecting distribution of Zygophyllum atriplicoides in semi-arid region of Iran (Case Study: Isfahan Province). *Desert* **20**, 145-156 (2015).

17 Caparros-Santiago, J. A., Rodriguez-Galiano, V. & Dash, J. Land surface phenology as indicator of global terrestrial ecosystem dynamics: A systematic review. *ISPRS Journal of Photogrammetry and Remote Sensing* **171**, 330-347, doi:https://doi.org/10.1016/j.isprsjprs.2020.11.019 (2021).

18 Zhu, W., Chen, G., Jiang, N., Liu, J. & Mou, M. Estimating Carbon Flux Phenology with Satellite-Derived Land Surface Phenology and Climate Drivers for Different Biomes: A Synthesis of AmeriFlux Observations. *PLOS ONE* **8**, e84990, doi:10.1371/journal.pone.0084990 (2013).

19 Bolton, D. K. *et al.* Continental-scale land surface phenology from harmonized Landsat 8 and Sentinel-2 imagery. *Remote Sensing of Environment* **240**, 111685, doi:https://doi.org/10.1016/j.rse.2020.111685 (2020).

20 White, M. A. *et al.* Intercomparison, interpretation, and assessment of spring phenology in North America estimated from remote sensing for 1982–2006. *Global Change Biology* **15** (2009).

21 Alimoradi, S., Khoorani, A. & Esmaeilpour, Y. Dynamics of Vegetation Cover in Relation to Temperature and Precipitation in the Rangelands of the Karun Basin, Khuzestan Province. *Applied Research in Geographical Sciences* **17**, 211-277 (2017).

22 Xie, Q. *et al.* Land surface phenology retrievals for arid and semi-arid ecosystems. *ISPRS Journal of Photogrammetry and Remote Sensing* **185**, 129-145, doi:https://doi.org/10.1016/j.isprsjprs.2022.01.017 (2022).

23 Moon, M. *et al.* Long-term continuity in land surface phenology measurements: A comparative assessment of the MODIS land cover dynamics and VIIRS land surface phenology products. *Remote Sensing of Environment* **226**, 74-92, doi:10.1016/j.rse.2019.03.034 (2019).

24 Tucker, C. J. Red and photographic infrared linear combinations for monitoring vegetation. *Remote Sensing of Environment* **8**, 127-150, doi:10.1016/0034-4257(79)90013-0 (1979).

25 Tong, X. *et al.* Trends of land surface phenology derived from passive microwave and optical remote sensing systems and associated drivers across the dry tropics 1992–2012. *Remote Sensing of Environment* **232**, 111307, doi:https://doi.org/10.1016/j.rse.2019.111307 (2019).

26 UNESCO. Islamic Republic of Iran, U. N. E., Scientific and Cultural Organization. Directory of the World Network of Biosphere Reserves (2015).

27 Ghasemi, S., Malekian, M., Tarkesh, M. & Rezvani, A. Climate change alters future distribution of mountain plants, a case study of Astragalus adscendens in Iran. *Plant Ecology* **223**, 1275-1288, doi:10.1007/s11258-022-01273-2 (2022).

28 Rezvani, A., Lorestani, N., Nematollahi, S., Hemami, M.-R. & Ahmadi, M. Should I stay or move? Quantifying landscape of fear to enhance environmental management of road networks in a highly transformed landscape. *Journal of Environmental Management* **368**, 122192, doi:10.1016/j.jenvman.2024.122192 (2024).

29 Soltani, S., Yaghmaei, L., Khodagholi, M. & Saboohi, R. Bioclimatic classification of Chahar-Mahal & Bakhtiari province using multivariate statistical methods. *Journal of Water and Soil Science* **14**, 53-68 (2011).

30 Piao, S. *et al.* Detection and attribution of vegetation greening trend in China over the last 30 years. *Global change biology* **21**, 1601-1609, doi:10.1111/gcb.12795 (2015).

31 Zhang, X. *et al.* Generation and evaluation of the VIIRS land surface phenology product. *Remote Sensing of Environment* **216**, 212-229, doi:10.1016/j.rse.2018.06.047 (2018).

32 Eklundh, L. & Jonsson, P.-G. in *Image and Signal Processing for Remote Sensing VIII.* (ed Sebastiano B. Serpico) 215-225.

33 Padhee, S. K. & Dutta, S. Spatio-Temporal Reconstruction of MODIS NDVI by Regional Land Surface Phenology and Harmonic Analysis of Time-Series. *GIScience & Remote Sensing* **56**, 1261-1288, doi:10.1080/15481603.2019.1646977 (2019).

34 Hird, J. N. & McDermid, G. J. Noise reduction of NDVI time series: An empirical comparison of selected techniques. *Remote Sensing of Environment* **113**, 248-258, doi:10.1016/j.rse.2008.09.003 (2009).

35 De Beurs, K. M. & Henebry, G. M. in *Phenological Research* (eds Irene L. Hudson & Marie R. Keatley) 177-208 (Springer Netherlands, 2010).

36 Forkel, M. & Wutzler, T. Greenbrown: land surface phenology and trend analysis. A package for the R software. Version 2.2. (2015).

37 Kendall, M. G. *Rank correlation methods*. 4th , 2d impression edn, viii, 202 pages : illustrations ; 24 cm (Griffin, 1975).

38 Sen, P. K. Estimates of the Regression Coefficient Based on Kendall's Tau. *Journal of the American Statistical Association* **63**, 1379-1389, doi:10.2307/2285891 (1968).

39 Xu, W., Hou, Y., Hung, Y. S. & Zou, Y. A comparative analysis of Spearman's rho and Kendall's tau in normal and contaminated normal models. *Signal Processing* **93**, 261-276, doi:https://doi.org/10.1016/j.sigpro.2012.08.005 (2013).

40 Kruskal, W. H. & Wallis, W. A. Use of Ranks in One-Criterion Variance Analysis. *Journal of the American Statistical Association* **47**, 583-621 (1952).

41 Masoudi, M., Asrari, E., Younesfard, A. R. & Haghighi, A. T. Spatial and Statistical Analysis of Climate Change in the Middle East: A Study of Precipitation and Temperature Variability Using NOAA Weather Data and Geostatistical Methods. *Earth Systems and Environment*, doi:10.1007/s41748-025-00802-z (2025).

42 Barnard, D. M., Barnard, H. R. & Molotch, N. P. Topoclimate effects on growing season length and montane conifer growth in complex terrain. *Environmental Research Letters* **12**, 064003 (2017).

43 Tomaszewska, M. A., Nguyen, L. H. & Henebry, G. M. Land surface phenology in the highland pastures of montane Central Asia: Interactions with snow cover seasonality and terrain characteristics. *Remote Sensing of Environment* **240**, 111675, doi:10.1016/j.rse.2020.111675 (2020).

44 Mozaffarian, V. *Flora of Chahar and Bakhtiari*. 1 edn, (Isfahan- Memar khane Baghnazar, 2017).

45 Pordel, F., Ebrahimi, A. & Azizi, Z. Evaluating spatio-temporal phytomass changes using vegetation index derived from Landsat 8 (Case study: Mrajan rangeland, Boroujen). *Rangeland* **11**, 166-178 (2017).

46 Thompson, J. A. & Paull, D. J. Assessing spatial and temporal patterns in land surface phenology for the Australian Alps (2000–2014). *Remote Sensing of Environment* **199**, 1-13, doi:10.1016/j.rse.2017.06.032 (2017).

47 Ipcc. Climate Change 2022: Impacts, Adaptation and Vulnerability. Chapter 10: Asia. (IPCC, 2022).

48 Pan, Y. *et al.* Climate-driven land surface phenology advance is overestimated due to ignoring land cover changes. *Environmental Research Letters* **18**, 044045, doi:10.1088/1748-9326/acca34 (2023).

49 Mohammadian, A., borujeni, E. A., Ebrahimi, A., Tahmasebi, p. & Naghipour, A. A. The combined effect of fire period and grazing intensity on plant species diversity indices in the semi-steppe rangeland of Chaharmahal and Bakhtiari province. *Iranian Journal of Range and Desert Research* **21**, 84-97 (2020).

50 Omidipour, R., Tahmasebi, P., Ebrahimi, A. & Nadaf, M. Investigating the Effect of Animal Grazing Management on Composition and Spatial Diversity Indices (Case Study: Broujen Rangelands, Charmahal and Bakhtiari). *Integrated Watershed Management Journal* **1**, 63-79 (2021).

51 Heidari Ghahfarrokhi, Z., Ebrahimi, A., Pordanjani, H. A., Asadi, E. & Shirmardi, H.-A. Effects of Livestock Grazing on Vegetation and Soil Properties in Rangelands: A Case Study of Farsan – Chaharmahal Va Bakhtiari Province. *Joournal of Rangeland* **17** (2024).

52 Qader, S. H., Priyatikanto, R., Khwarahm, N. & Tatem, A. Characterising the land surface phenology of middle eastern countries using moderate resolution landsat data. (2022).

53 Khormizi, H. Z., Malamiri, H. R. G., Kalantari, Z. & Ferreira, C. S. S. Trend of Changes in Phenological Components of Iran's Vegetation Using Satellite Observations. *Remote Sensing* **15**, 1-21, doi:10.3390/rs15184468 (2023).

54 Vogel, J. Drivers of phenological changes in southern Europe. *International Journal of Biometeorology* **66**, 1903-1914, doi:10.1007/s00484-022-02331-0 (2022).

55 Mirgol, B. *et al.* Interplay Among Recent Trends in Climate Extremes, Vegetation Phenology, and Crop Production in the Southern Mediterranean Region. *International Journal of Climatology* **45**, e8768, doi:https://doi.org/10.1002/joc.8768 (2025).

56 Wipf, S., Stoeckli, V. & Bebi, P. Winter climate change in alpine tundra: plant responses to changes in snow depth and snowmelt timing. *Climatic Change* **94**, 105-121, doi:10.1007/s10584-009-9546-x (2009).

57 An, S., Zhang, X. & Ren, S. Spatial Difference between Temperature and Snowfall Driven Spring Phenology of Alpine Grassland Land Surface Based on Process-Based Modeling on the Qinghai–Tibet Plateau. *Remote Sensing* **14**, 1273 (2022).

58 Liu, Y., Zhou, W., Gao, S., Ma, X. & Yan, K. Phenological Responses to Snow Seasonality in the Qilian Mountains Is a Function of Both Elevation and Vegetation Types. *Remote Sensing* **14** (2022).

59 Garonna, I. *et al.* Shifting relative importance of climatic constraints on land surface phenology. *Environmental Research Letters* **13**, 024025, doi:10.1088/1748-9326/aaa17b (2018).

60 Zhumanova, M., Wrage-Mönnig, N. & Jurasinski, G. Long-term vegetation change in the Western Tien-Shan Mountain pastures, Central Asia, driven by a combination of changing precipitation patterns and grazing pressure. *Science of The Total Environment* **781**, 146720, doi:10.1016/j.scitotenv.2021.146720 (2021).

61 Dronova, I. & Taddeo, S. Remote sensing of phenology: Towards the comprehensive indicators of plant community dynamics from species to regional scales. *Journal of Ecology* **110**, 1460-1484, doi:https://doi.org/10.1111/1365-2745.13897 (2022).

62 Iwanycki Ahlstrand, N., Primack, R. B. & Tøttrup, A. P. A comparison of herbarium and citizen science phenology datasets for detecting response of flowering time to climate change in Denmark. *International Journal of Biometeorology* **66**, 849-862, doi:10.1007/s00484-022-02238-w (2022).

63 Eyshi Rezaei, E., Siebert, S. & Ewert, F. Climate and management interaction cause diverse crop phenology trends. *Agricultural and Forest Meteorology* **233**, 55-70, doi:https://doi.org/10.1016/j.agrformet.2016.11.003 (2017).

64 Park, D. S., Newman, E. A. & Breckheimer, I. K. Scale gaps in landscape phenology: challenges and opportunities. *Trends in Ecology & Evolution* **36**, 709-721, doi:https://doi.org/10.1016/j.tree.2021.04.008 (2021).

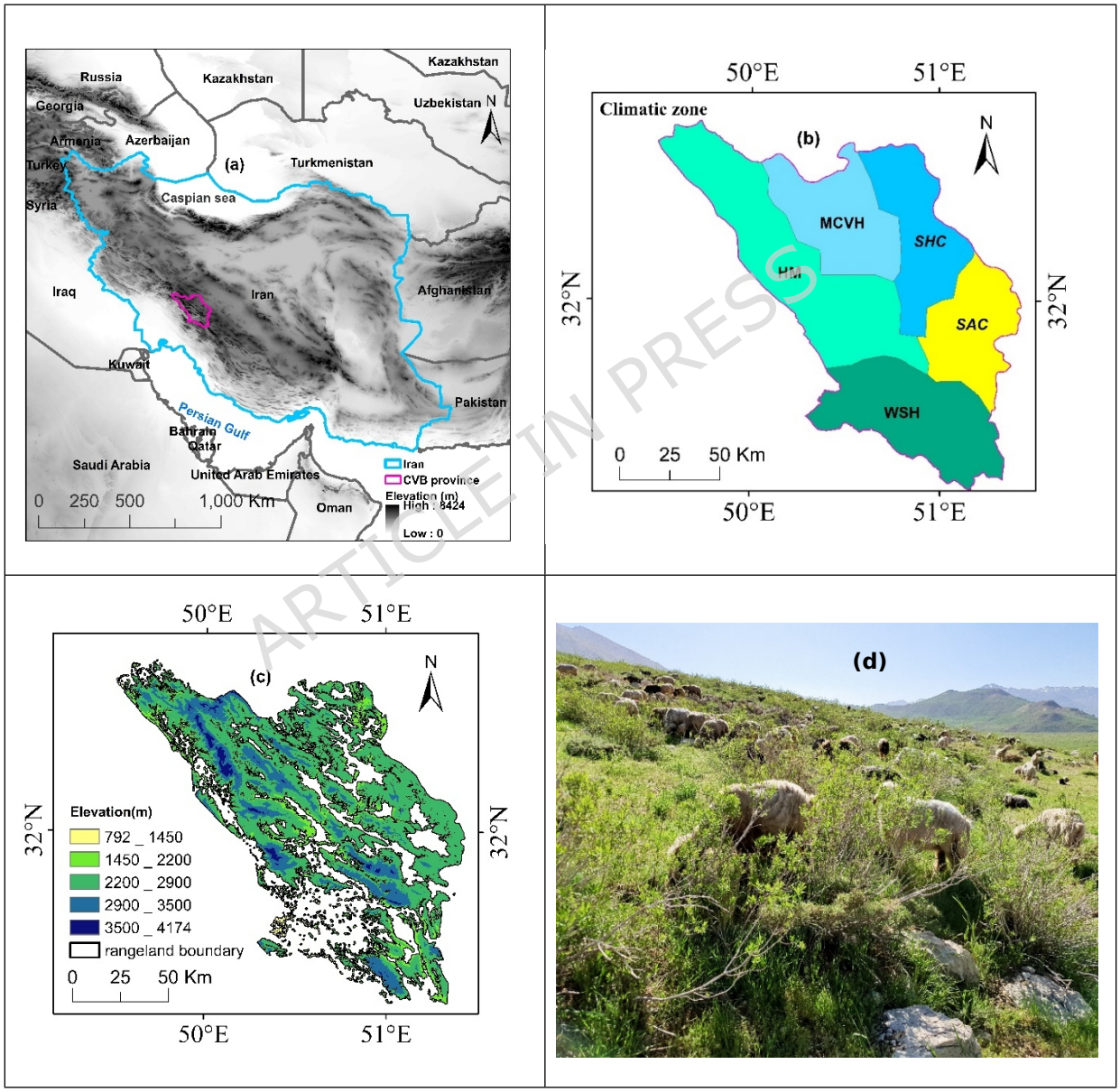

Figure. 1. (a) Location of Chaharmahal-Va-Bakhtiari (CVB) province in Iran; (b) climatic classification map showing different climate zones**:** MCVH (mountainous

cold and very humid), SHC (semi-humid and cold), SAC (semi-arid and cold), HM (humid and moderate), and WSH (warm and semi-humid); (c) an elevation map (rangelands filled with white colour); and (d) a sample photo of vegetation cover within the study area (Maps were generated using ArcMap 10.5).

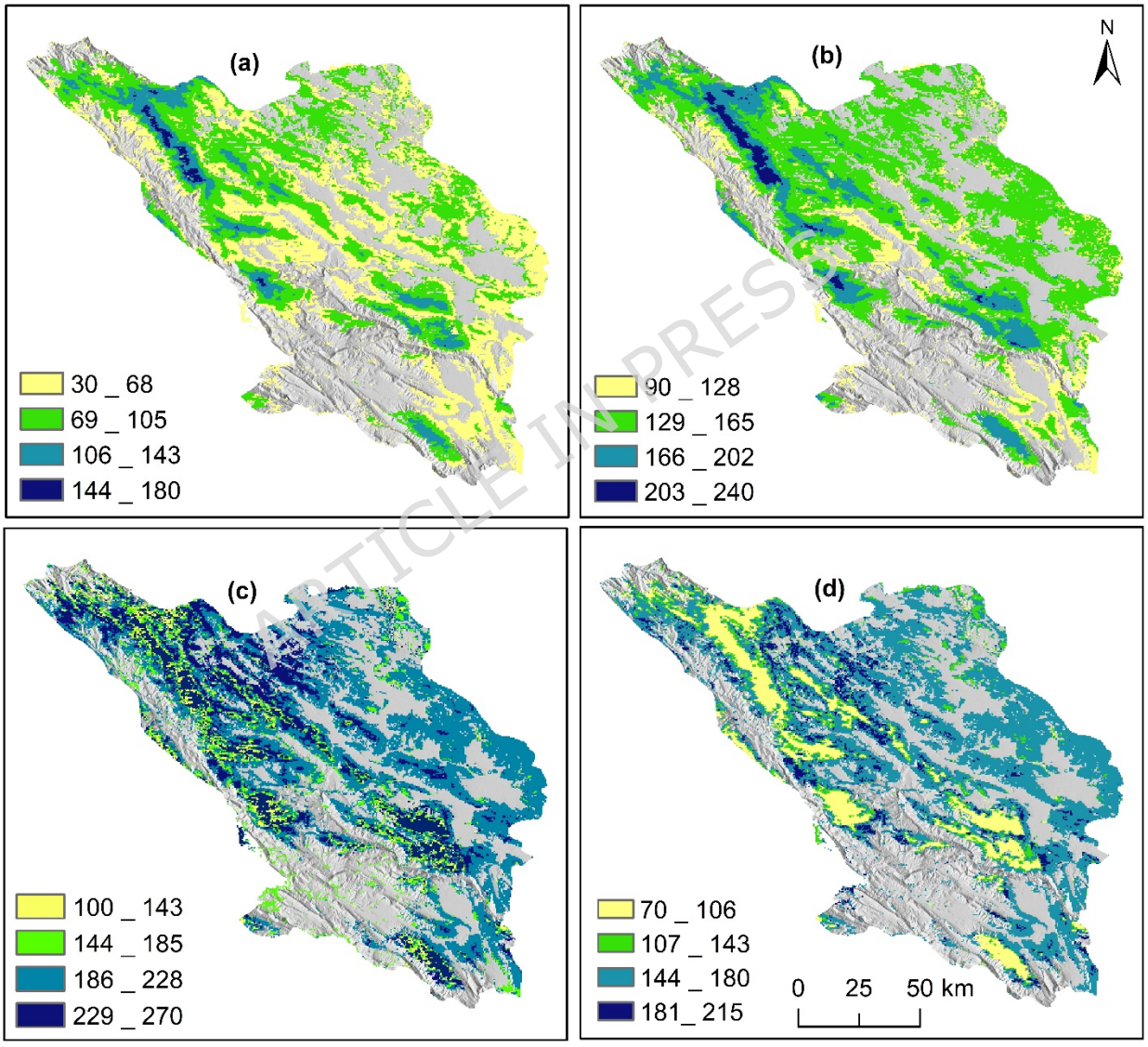

Figure. 2. Spatial distribution of average phenometrics from 2000 to 2023 reported in day of the year (DOY) ranges for (a) start of the growing season (SOS), (b) peak of the growing season (POS), (c) end of the growing season (EOS), or number of days

for (d) length of the growing season (LOS). Each class represents one quartile of the range of numerical values in the map. Areas without rangelands filled with gray colour (Maps were generated using ArcMap 10.5).

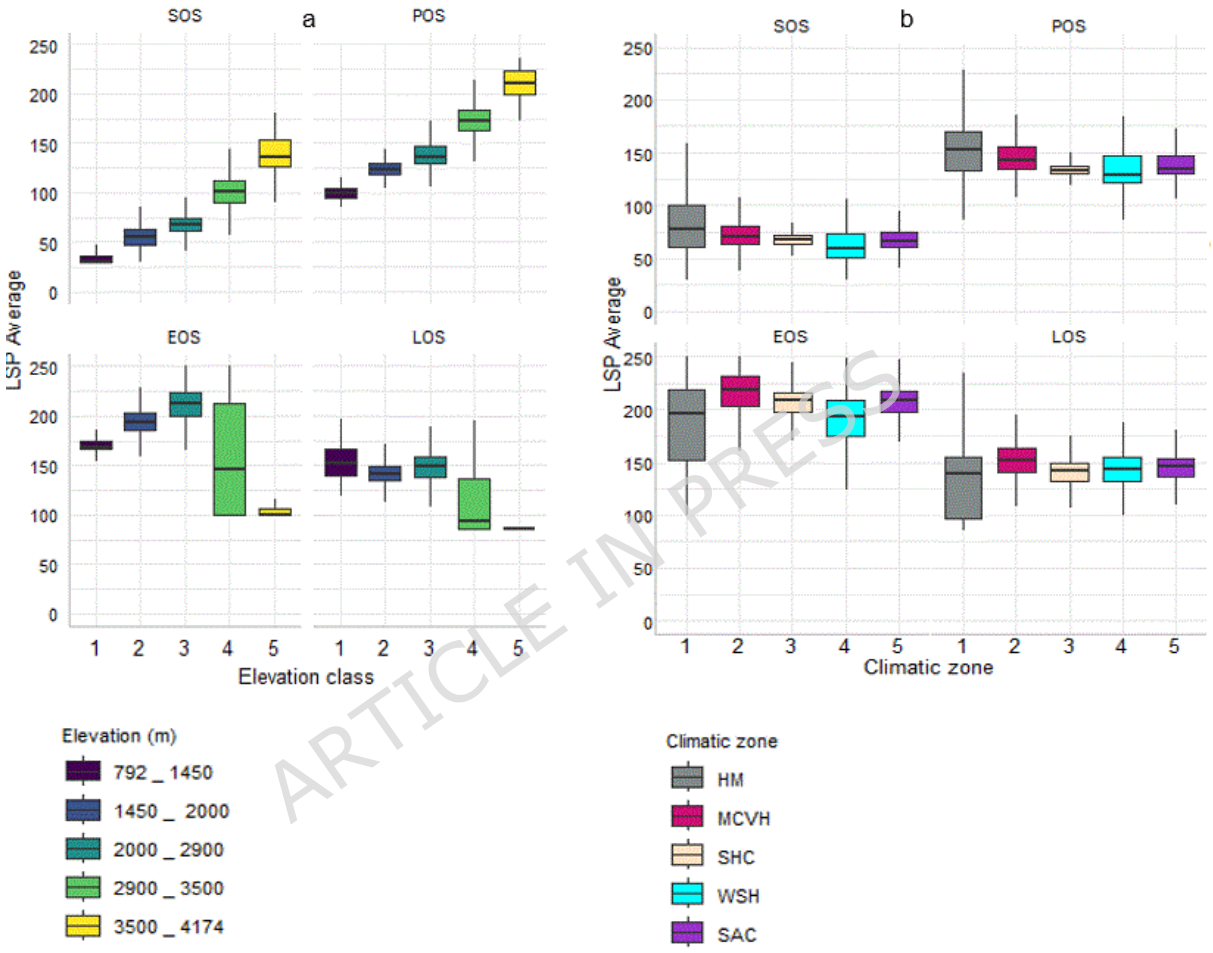

Figure. 3. Evaluating the influence of (a) elevation and (b) climatic zone on the average of phenometrics from 2000 to 2023 (a Kruskal-Wallis analysis of start of the growing season (SOS), peak of the growing season (POS), end of the growing season (EOS), and length of the growing season (LOS) with p-value ≤ 0.05). The line inside each box represents the median, while the bottom and top of the box indicate the first quartile and third quartile, respectively.

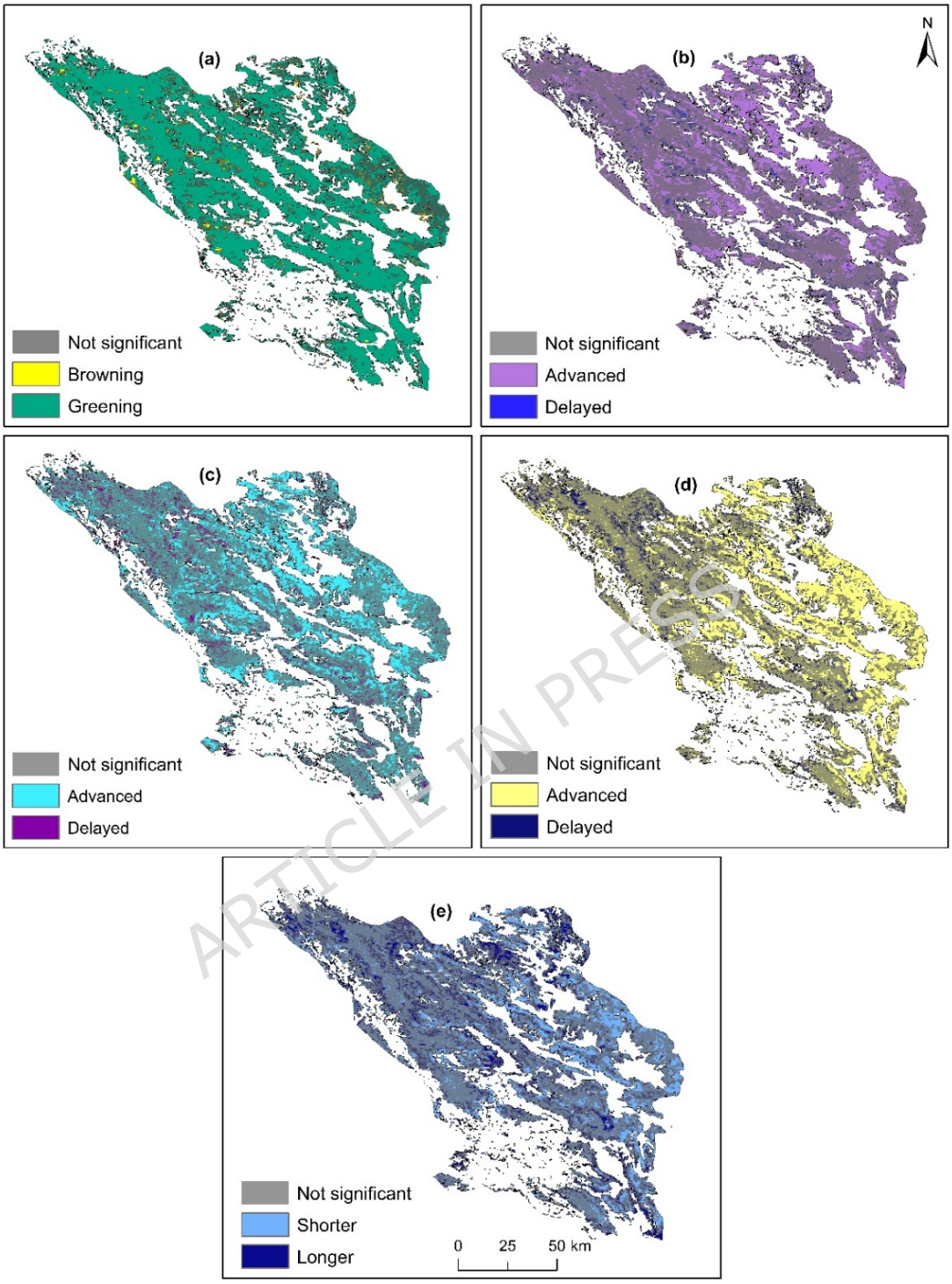

Figure. 4. Spatial-temporal slope trends of phenology metrics from 2000 to 2023: (a) max-NDVI, (b) start of the growing season (SOS), (c) peak of the growing season (POS), (d) end of the growing season (EOS), and (e) length of the growing season

(LOS). Areas without rangelands appear white (Maps were generated using ArcMap 10.5).

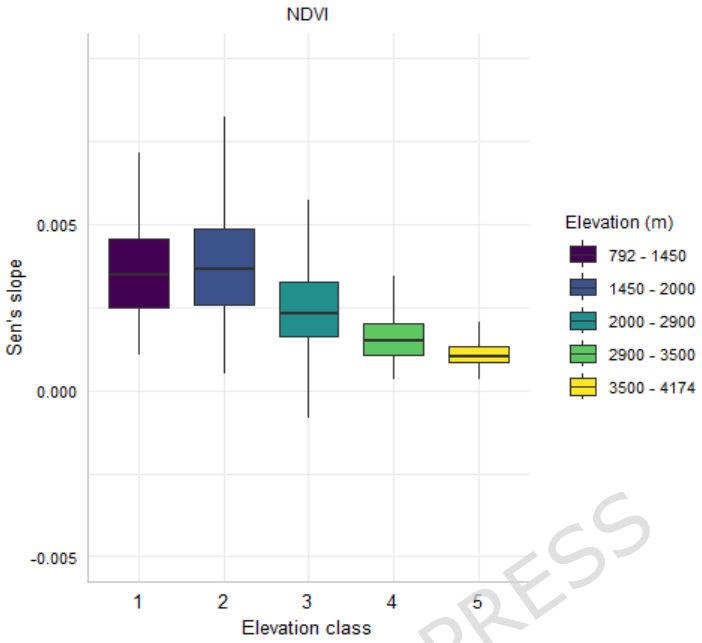

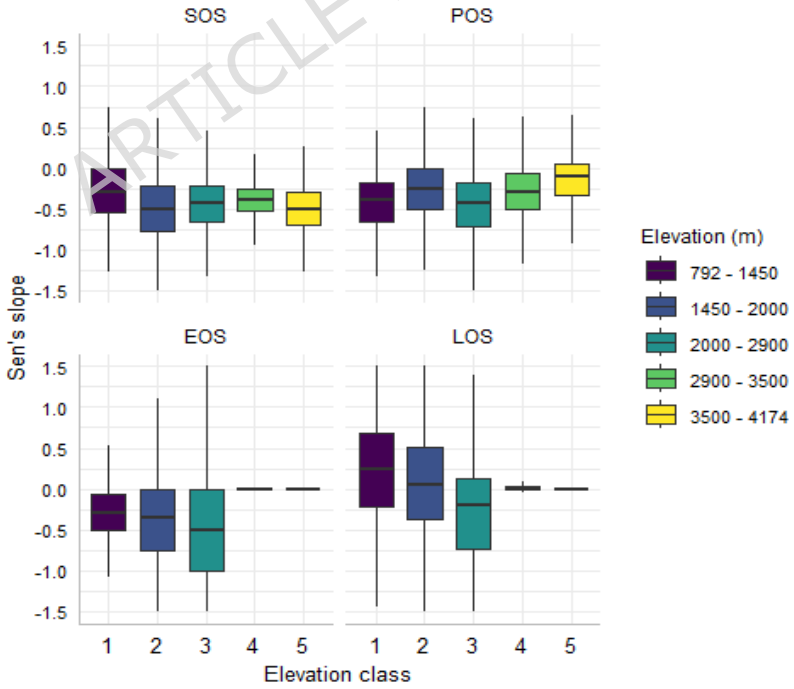

Figure. 5. Elevation-based Kruskal-Wallis analysis of Sen's slope for NDVI, start of the growing season (SOS), peak of the growing season (POS), end of the growing season (EOS), and length of the growing season (LOS) (p-value ≤ 0.05). The line inside each box represents the median, while the bottom and top of the box indicate the first quartile and third quartile, respectively.

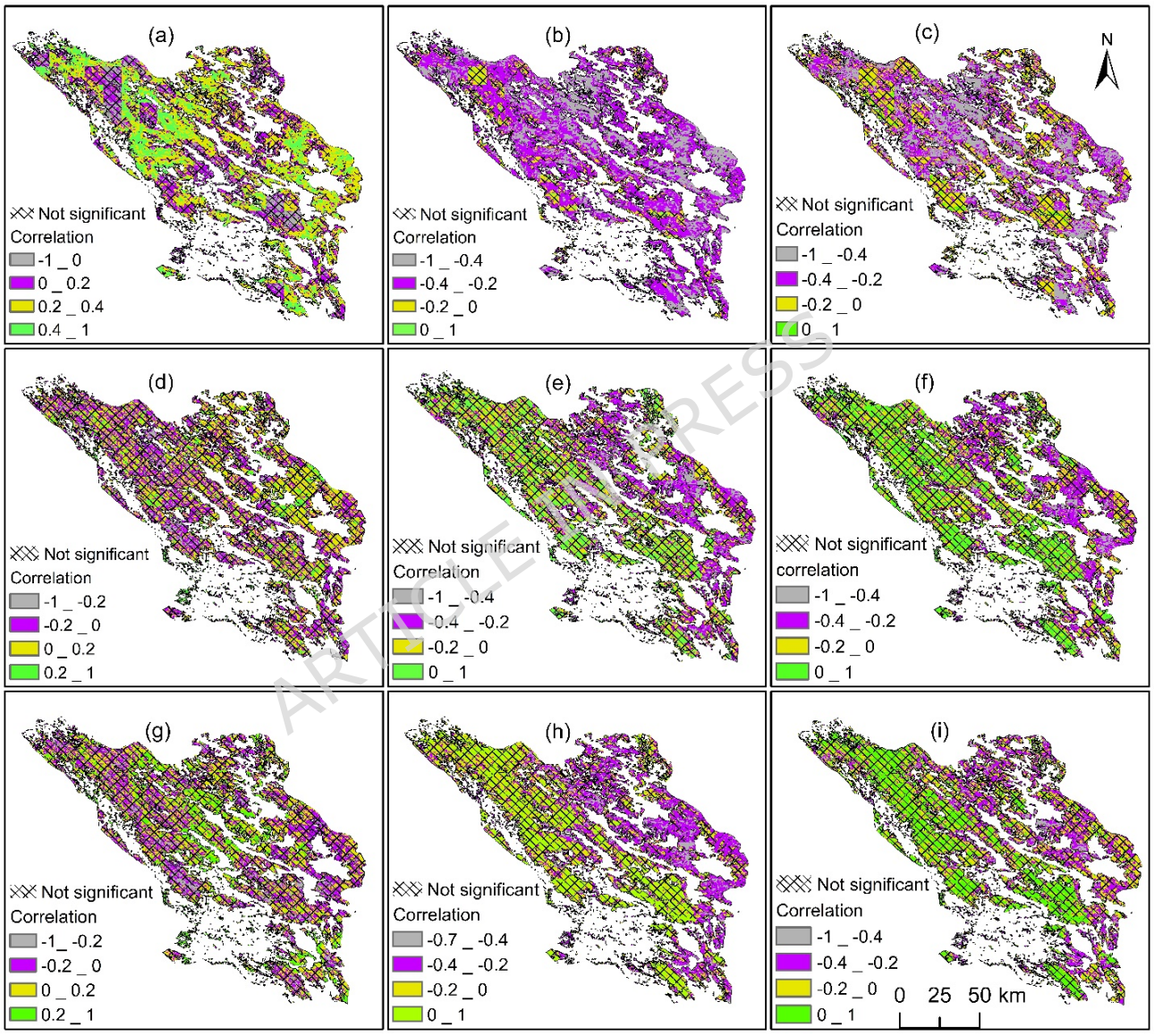

Figure. 6. Spatial distribution of Kendall's correlation coefficient between the land surface phenology (LSP) metrics and climate variables in the study area during 2000-2023: (a) Pre-SOS total precipitation, (b) Pre-SOS mean temperature, (c) Pre-

SOS mean PET, (d) Pre-EOS total precipitation, (e) Pre-EOS mean temperature, (f) Pre-EOS mean PET, (g) Growing season precipitation, (h) Growing season temperature, and (i) Growing season PET (Maps were generated using ArcMap 10.5).

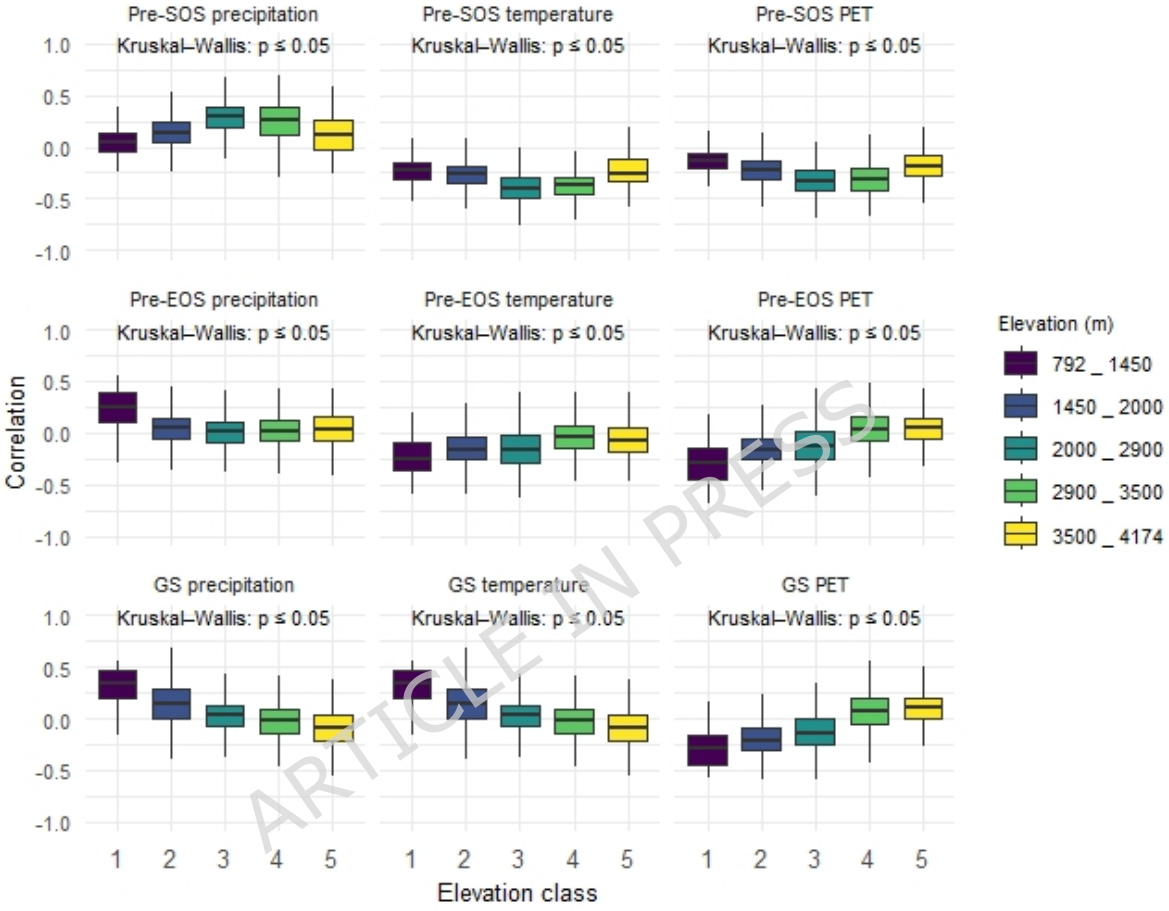

Figure. 7. Elevation-based Kruskal-Wallis analysis of Kendall's correlation coefficient between the land surface phenology (LSP) metrics and climate variables in the study area during 2000-2023 (p-value ≤ 0.05). The line inside each box represents the median, while the bottom and top of the box indicate the first quartile and third quartile, respectively.

Figure captions

Figure. 1. (a) Location of Chaharmahal-Va-Bakhtiari (CVB) province in Iran; (b) climatic classification map showing different climate zones**:** MCVH (mountainous cold and very humid), SHC (semi-humid and cold), SAC (semi-arid and cold), HM (humid and moderate), and WSH (warm and semi-humid); (c) an elevation map (rangelands filled with white colour); and (d) a sample photo of vegetation cover within the study area (Maps were generated using ArcMap 10.5).

Figure. 2. Spatial distribution of average phenometrics from 2000 to 2023 reported in day of the year (DOY) ranges for (a) start of the growing season (SOS), (b) peak of the growing season (POS), (c) end of the growing season (EOS), or number of days for (d) length of the growing season (LOS). Each class represents one quartile of the range of numerical values in the map. Areas without rangelands filled with gray colour (Maps were generated using ArcMap 10.5).

Figure. 3. Evaluating the influence of (a) elevation and (b) climatic zone on the average of phenometrics from 2000 to 2023 (a Kruskal-Wallis analysis of start of the growing season (SOS), peak of the growing season (POS), end of the growing season (EOS), and length of the growing season (LOS) with p-value ≤ 0.05). The line inside each box represents the median, while the bottom and top of the box indicate the first quartile and third quartile, respectively.

Figure. 4. Spatial-temporal slope trends of phenology metrics from 2000 to 2023: (a) max-NDVI, (b) start of the growing season (SOS), (c) peak of the growing season (POS), (d) end of the growing season (EOS), and (e) length of the growing season (LOS). Areas without rangelands appear white (Maps were generated using ArcMap 10.5).

Figure. 5. Elevation-based Kruskal-Wallis analysis of Sen’s slope for NDVI, start of the growing season (SOS), peak of the growing season (POS), end of the growing season (EOS), and length of the growing season (LOS) (p-value ≤ 0.05). The line

inside each box represents the median, while the bottom and top of the box indicate the first quartile and third quartile, respectively.

Figure. 6. Spatial distribution of Kendall's correlation coefficient between the land surface phenology (LSP) metrics and climate variables in the study area during 2000-2023: (a) Pre-SOS total precipitation, (b) Pre-SOS mean temperature, (c) Pre-SOS mean PET, (d) Pre-EOS total precipitation, (e) Pre-EOS mean temperature, (f) Pre-EOS mean PET, (g) Growing season precipitation, (h) Growing season temperature, and (i) Growing season PET (Maps were generated using ArcMap 10.5).

Figure. 7. Elevation-based Kruskal-Wallis analysis of Kendall's correlation coefficient between the land surface phenology (LSP) metrics and climate variables in the study area during 2000-2023 (p-value ≤ 0.05). The line inside each box represents the median, while the bottom and top of the box indicate the first quartile and third quartile, respectively.